Hybrid Quantum Interferometer in Bifurcation Mode as a Latching Quantum Readout

Connor D. Shelly[1,2,*,†] Christopher Checkley,[1] and Victor T. Petrashov[1]

[1]*Royal Holloway, University of London, Egham TW20 0EX, United Kingdom*
[2]*National Physical Laboratory, Hampton Road, Teddington TW11 0LW, United Kingdom*

We develop a type of magnetometer consisting of a hybrid quantum interference device (HyQUID) that is set in a bistable state. We demonstrate its operation in a latching mode that can be employed to measure small changes in the applied flux. The device can be used to probe the flux state of a superconducting circuit using straightforward electrical resistance measurements, making it suitable as a simple qubit readout with low back action.

I. INTRODUCTION

The ability to detect extremely small changes in magnetic flux is of paramount importance in a number of applications. One area of particular interest is the readout of superconducting flux qubits. Here, it is necessary that the detector is not only able to measure extremely small changes in the flux generated by the qubit but also that it has minimal back action so that it does not induce quantum decoherence.

The quantum state of the qubit can be determined by measurement of the magnetic flux in the system. Typically a superconducting quantum interference device (SQUID) has been used to achieve this [1].

Existing SQUID-based readout methods of the state of a qubit are unsatisfactory for a number of reasons. First, to produce a readout, the SQUID is switched into a finite-voltage state, a process that strongly disturbs both the qubit circuit and the SQUID itself. Bursts of nonequilibrium quasiparticles are created, with energies exceeding the superconductor gap, thus "poisoning" the qubit circuit and leading to decoherence [2]. Second, due to the ac Josephson effect, the voltage across the SQUID produces a microwave voltage pulse that can drive neighboring qubits into their excited states [3]. While being useful for proof-of-principle purposes, switching methods are unsuitable for simultaneous measurements of multiple qubits or experiments in which the preservation of the qubit state after the measurement is required (e.g., quantum nondemolition measurements [4]).

In an effort to overcome the above problems, an alternative readout device has been developed—the Josephson bifurcation amplifier (JBA) [5]. The JBA is essentially a nonlinear oscillator formed by a capacitively shunted Josephson junction. The JBA uses a dispersive measurement technique to avoid switching of the junction into a finite-voltage state. The principle of the measurement technique is to drive the system with a sufficiently large rf excitation while measuring the plasma frequency response [4,6]. This high drive power causes the oscillator to enter a nonlinear regime in which a bistability occurs [7]. As the plasma frequency response also varies with the critical current of the junction, it is possible to use the JBA as a sensitive threshold detector. A particular advantage of this measurement technique is that the JBA will remain in the same state post measurement, which allows the system to be employed as a latching readout of superconducting circuits such as flux qubits [8,9]. Although the JBA addresses a number of the shortcomings of SQUID-based measurements, there are still disadvantages to the method, namely the necessity for a large-amplitude electromagnetic field in the system. The necessary coupling to the resonant cavity can also lead to photon-induced dephasing of the qubit [10,11]. Finally, in order to properly drive the JBA, a complicated and expensive arrangement of transmission lines, circulators, and rf electronics is required.

Hybrid quantum interference devices (HyQUIDs) are hybrid mesoscopic devices that act as sensitive detectors of superconducting phase [12–14]. In this paper, we show how a HyQUID can be set in a bistable state exhibiting a similar latching action to the JBA. This can be achieved without the need for the aforementioned complicated rf equipment—instead, only the measurement of a quasi-dc voltage is needed to perform the HyQUID readout.

* Corresponding author. cshelly@oxfordquantumcircuits.com
† Present address: Oxford Quantum Circuits, Thames Valley Science Park, Shinfield, Reading RG2 9LH, United Kingdom.

II. THE HYBRID QUANTUM INTERFERENCE DEVICE

A. HyQUID operation principles

The HyQUID consists of a superconducting loop interrupted by a normal-conductor weak link. A scanning electron micrograph and device schematics are shown in Fig. 1. The normal cross of the HyQUID makes contact with normal electrodes at points (a) and (b) and with the superconducting loop at points (c) and (d). The electrical resistance of the interferometer between points (a) and (b) oscillates as a function of the superconducting phase difference $\phi = \phi_1 - \phi_2$ between points (c) and (d) and is described by

$$\Delta R_N = \gamma[1 - \cos(\phi)], \tag{1}$$

where γ is an amplitude factor controlled by properties of the system, such as the quality of the superconductor–normal-metal (S-N) interface, and depends on the relation between the lengths of the normal conductor $L_{c\text{-}d}$ connecting the superconductors and on characteristic length scales such as the electron phase-breaking length $L_\varphi = \sqrt{D\tau_\varphi}$ and the coherence length $\xi_N = \sqrt{\hbar D/2\pi k_B T}$, where τ_φ is the phase-breaking time and D is the diffusion coefficient.
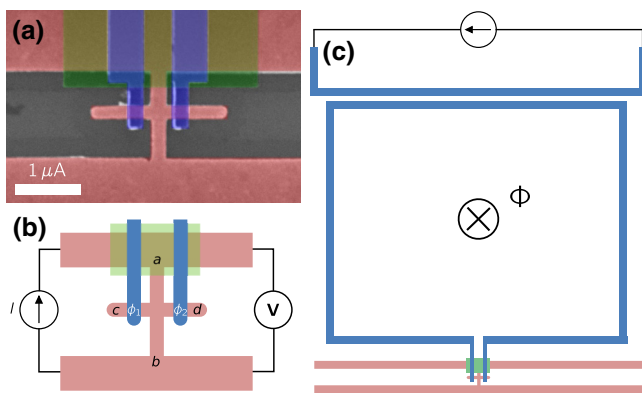

FIG. 1. (a) A scanning electron micrograph of the HyQUID cross. The silver layer (normal metal) is colored red, the aluminum layer (superconductor) is colored blue, and the silicon monoxide layer (insulating spacer) is colored green. (b) A circuit schematic showing the HyQUID cross. One branch of the cross is connected to two normal-metal reservoirs—a four-point measurement is used to monitor the resistance of the cross. The resistance of the normal branch oscillates as a function of the phase difference between the two superconductors $\phi = \phi_1 - \phi_2$. (c) A schematic demonstrating the principle of operation of the HyQUID. The superconducting electrodes are joined to form a loop. A magnetic flux Φ can be applied to the loop using either an on-chip flux line (shown) or an external solenoid. The flux changes the phase difference across the interferometer and the resulting change in the HyQUID resistance is measured.

Due to the proximity effect, a superconducting Josephson current can be induced in the normal segment of the HyQUID, with a critical value that depends on the distance between the two superconducting contacts, $L_{c\text{-}d}$. Figure 2(a) shows that as the distance between the superconducting contacts is increased, the critical current of the S-N-S junction reduces. This allows specific critical current values to be designed during the fabrication stage. It is also possible to modify the critical current of the S-N-S junction by applying a control current between the two normal reservoirs. Figure 2(b) shows the dependence of the critical current of a S-N-S junction on the applied bias current I_N, allowing full suppression of I_c and thus control of the critical current during an experiment. The suppression of I_c is due to the control of the quasiparticle distribution over the supercurrent-carrying Andreev states [15]. For the HyQUID used in this work, we design and fabricate the device parameters such that we are in the range $L_{c\text{-}d} < \xi_N, L_\phi$. This allows us to modify the behavior of the HyQUID during the experiment and access different operating regimes.

B. HyQUID fabrication and measurement setup

Figures 1(a) and 1(b) show a scanning electron micrograph and circuit schematic of the interferometer described in this paper. The patterns are defined using standard electron-beam-lithography techniques. The normal and superconducting materials used are Ag and Al, respectively. Both are deposited using thermal evaporation. In order to ensure a good interface between the two metals, an *in situ* argon etch is used.
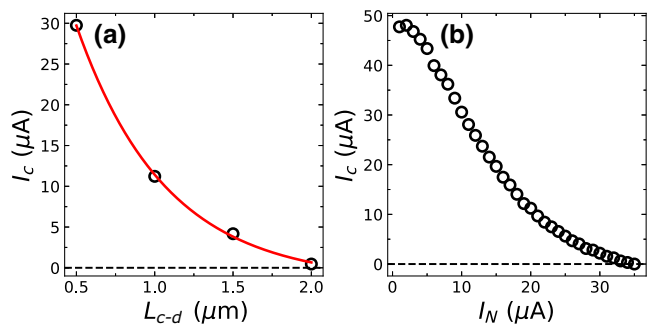

FIG. 2. (a) The black open circles show the measured critical current as a function of $L_{c\text{-}d}$ for superconductor–normal-metal–superconductor (S-N-S) junctions with different values of $L_{c\text{-}d}$. The critical current reduces as the length of the S-N-S junction is increased. The red line shows a fit to $I_c \propto \exp(-L_{c\text{-}d}/\xi)$ from which an estimate of the coherence length can be made, $\xi \approx 570$ nm. (b) The black open circles show the measured critical current of the S-N-S junction with an increasing bias current I_N applied between the two normal reservoirs. The applied bias current I_N provides control of the critical current I_c.

The S-N-S junction is 200 nm wide and 50 nm thick and the distance between the two S contacts, $L_{c\text{-}d} = 500$ nm. The distance between the two N reservoirs, $L_{a\text{-}b} = 2000$ nm. Using a simple approximation for a square loop, we estimate the geometric inductance of the loop to be $L \approx 100$ pH. All measurements are conducted in a ^{3}He cryostat with a base temperature of 280 mK. The resistance of the interferometer is measured using standard lock-in amplifier techniques. The magnetic flux through the interferometer Φ is controlled using both a superconducting solenoid in the cryostat and an on-chip flux line for pulsed measurements. The pulses are controlled using an arbitrary waveform generator. To modify the critical current, we apply a dc current I_N between the two N reservoirs, so that $V_N = I_N R_N$. We measure a normal-state resistance $R_N = 2.8\ \Omega$ at 280 mK. The diffusion constant is estimated from similar fabricated devices (see Refs. [14,16]) to be $D \approx 0.08\ \mathrm{m^2\,s^{-1}}$. Using the theory presented in Ref. [16], we estimate $L_\phi > 3\ \mu$m. Several interferometers are fabricated, all showing similar behavior.

III. THE HyQUID IN BIFURCATION MODE

A. HyQUID dynamics

Past investigations of hybrid normal-superconducting interferometers have focused on the range in which $\xi_N < L_{c\text{-}d} < L_\phi$. In this regime, the Josephson screening current in the flux-sensitive loop of the interferometer is negligible. The phase-periodic oscillations in this regime are sinusoidal (or cusplike), as shown in Fig. 3(b), and the phase-flux relationship is single valued, as shown in Fig. 3(d).

In this work, we investigate the HyQUID with $L_{c\text{-}d}$, which is smaller than both the phase-breaking length and the coherence length; $L_{c\text{-}d} < \xi_N, L_\phi$. In this regime, the Josephson screening current is created with finite critical current I_c, changing the behavior of the HyQUID drastically. The dynamics can be described using the resistively and capacitively shunted Josephson junction (RCSJ) model [17,18]. The dependence of the potential energy of our system is described by

$$U = E_J \left[1 - \cos\phi + \frac{(\phi - \phi_e)^2}{2\beta} \right], \qquad (2)$$

where ϕ_e is the externally applied phase, $E_J = I_c \Phi_0 / 2\pi$ is the Josephson energy, $\beta = 2\pi L I_c / \Phi_0$ is the screening parameter, and L is the geometric inductance of the loop.

The potential energy of the system can therefore be modified by control of β (through varying the dc current I_N) and through control of the external phase ϕ_e applied to the HyQUID. At large values of β (large critical currents), there are several stable states corresponding to minima in the local potential energy. At small values of β (small critical currents), the system has only one stable minimum.
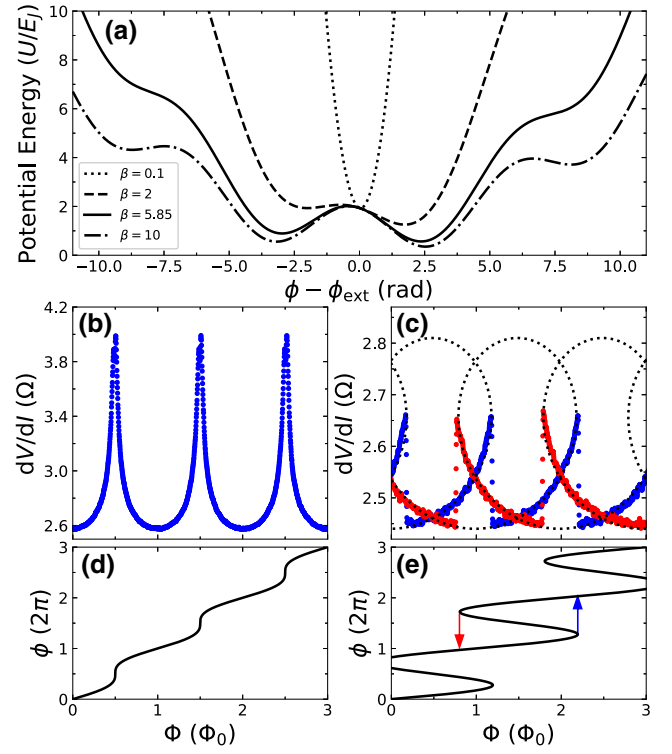

FIG. 3. (a) The potential energy of the HyQUID [see Eq. (2)] for different values of β. By varying β, the number and position of minima can be controlled. (b),(c) The differential resistance of the interferometer as a function of the applied flux Φ for $I_N = 30\ \mu$A ($\beta = 4.95$) and $I_N = 50\ \mu$A ($\beta = 1$), respectively. The blue data show the differential resistance when the flux is swept in the positive direction and the red data when flux is swept in a negative direction. The black dotted line is a fit to theory using Eqs. (1) and (3), showing the unstable regions of the curve. (d),(e) The phase across the interferometer ϕ as a function of the applied magnetic flux Φ, calculated using the values of β determined from (b) and (c), respectively. The blue and red arrows show the points where the phase switches between branches.

Figure 3(a) shows the potential energy of the HyQUID for different values of β. The dynamics of such a system can be experimentally observed by measuring the differential resistance of the interferometer at different values of β.

The Josephson screening current is created with a finite critical current I_c and the phase ϕ is related to the magnetic flux threading the loop by

$$2\pi \Phi / \Phi_0 = \phi + \beta \sin\phi. \qquad (3)$$

As β is increased, the relationship between ϕ and Φ becomes increasingly nonlinear and at $\beta > 1$ it becomes multivalued. At the points shown by arrows in Fig. 3(e), the system can exist in two different states (bifurcation). Figures 3(c) and 3(e) show the operating regime that is discussed in this paper. When $\beta > 1$, the phase as a function

of applied flux is multivalued—initially, the superconducting phase starts on one branch with a positive gradient. As the flux approaches a critical value, the gradient changes sign. Beyond this critical flux, the gradient becomes negative. The negative gradient represents values of phase that are unstable and thus the phase jumps to the next branch with a positive gradient. This results in dynamics that are path dependent (in our case, flux-sweep-direction dependent). The differential resistance as a function of the applied flux is shown in Fig. 3(c). The blue data are the positive flux sweep and the red data are the negative flux sweep. The blue and red arrows on the phase-flux diagram of Fig. 3(e) represent the corresponding points where the phase switches between branches. It should be noted that the two regimes shown [Figs. 3(b) and 3(c)] are measured using the same HyQUID. Only the applied dc current I_N is used to tune between these regimes. The full range of HyQUID differential resistance behavior is shown in the Appendix.

The differential resistance close to the bistable points shows an extreme sensitivity to the applied flux [as per Fig. 3(c)]. This happens because the height of the potential energy barrier keeping the system in the local potential well becomes small enough for the system to escape the well. As can be seen from Eq. (2), the escape can be stimulated by manipulation of external flux or, alternatively, by manipulation of β via applied dc current I_N [as per Fig. 3(a)]. The differential resistance as a function of the bias current I_N is shown in Fig. 4. In this control protocol, the applied flux to the HyQUID is fixed and the bias current I_N is swept. Similar to the protocol of Fig. 3, the dynamics arise as a result of instabilities of the phase-flux diagram. In this case, the value of β varies as I_N is varied; therefore, the form of the phase-flux dependence varies as I_N is varied.

As I_N is increased, β reduces. As β is reduced, the phase-flux diagram tends toward linear. For a fixed applied flux as shown in Fig. 4(a), the HyQUID phase increases as I_N is increased. At some value of I_N, the phase becomes unstable and a phase jump to the next branch occurs. The phase progression as I_N is varied is shown in Figs. 4(a) and 4(b). The blue arrows represent the path when I_N is increased. The red arrows represent the path when I_N is decreased. By considering the differential resistance of the HyQUID in this regime, we again find that a hysteretic behavior is observed [Fig. 4(c)], which allows the HyQUID to be used as a latched readout device. The experimental dependence of the differential resistance as a function of I_N for our device is shown in Fig. 4(d) and agrees qualitatively with the modeled data.

B. Latching readout

As described in the previous sections, the high sensitivity of the HyQUID to small changes in flux and/or bias
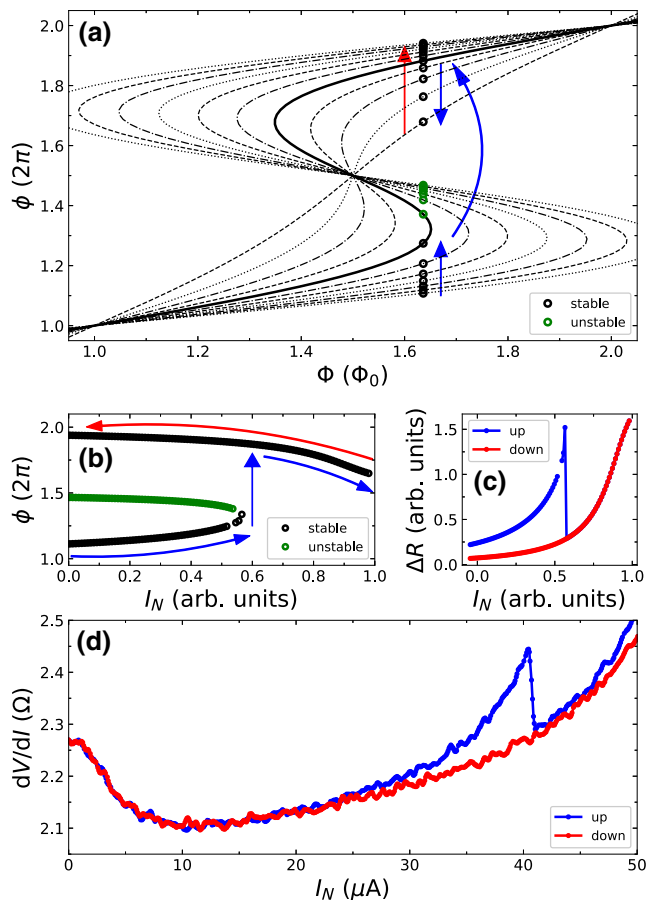

FIG. 4. (a) The phase-flux diagram for multiple values of β. For clarity, only a subset of curves are shown. The external flux is fixed ($\Phi = 1.64\Phi_0$) and the phase ϕ is found for each β by solving Eq. (3). Some of the phase solutions occur on negative gradients (green open circles) and are unstable. Only the stable solutions (black open circles) are experimentally accessible. The path dependence of the dynamics is illustrated on the graph; as the bias current is increased (β decreased), the phase increases until a negative gradient of the phase-flux curve is reached (this occurs on the solid black curve). The phase then jumps to the next stable level and then progresses smoothly again. This can be observed by following the blue arrows on the graph. The red arrow represents the phase progression as the bias current is reduced (β increased). (b) The phase as a function of the applied dc current. As the current is increased, a jump in the phase is observed. (c) This phase jump is then observed in the calculated differential resistance of the HyQUID [Eq. (1)]. A clear path dependence is observed based on the direction of the bias-current sweep. (d) The experimental differential resistance data as a function of the applied dc bias current: blue is the *up* current sweep and red is the *down* current sweep. The behavior of the HyQUID during the experiment follows the model presented in (a)–(c).

current at the bifurcation points can be used for the construction of a latching amplifier that can be used for the readout of quantum circuits, such as superconducting flux qubits.

To use the HyQUID as a latching readout, we take advantage of the bistability in the HyQUID dynamics and implement pulsed measurements using two alternative protocols for manipulation of the flux and bias current.

1. Latching readout using flux manipulation

The readout protocol is shown in Fig. 5. The applied flux Φ_{ext} to the HyQUID is controlled via an on-chip flux line. The dc current I_N is added to the small ac current used for lock-in detection. Both pulses are controlled using an arbitrary waveform generator. We again use the RCSJ model description of our system and use the pulsed protocol to control the "particle" in a potential energy well. The system is initialized so that the particle sits in a single lower well [Fig. 5(c-i)]. By increasing the applied flux, the well is raised [Fig. 5(c-ii)], trapping the particle. A short flux pulse Φ_{step} is applied for time Δt, temporarily lowering the barrier between the two wells [Fig. 5(c-iii)], allowing for the possibility that the particle escapes to the other well—this leads to a sudden change in phase (which manifests as a change to the HyQUID resistance). The barrier is reinstated by reducing the applied flux and a measurement of the HyQUID resistance is made—due to the

latching nature of operation, this measurement determines whether or not the particle escapes [Fig. 5(c-iv)]. Finally, the system is reset by removing the flux and current bias [Fig. 5(c-v)].

During stage (iii) of the measurement protocol, the barrier is reduced and the particle has some possibility of escaping the lower well. The escape rate from the potential well is written as

$$\Gamma = \frac{\omega}{2\pi} \exp[-U_0/k_B T], \quad (4)$$

where ω is the escape-attempt frequency and U_0 is the barrier height [19,20]. For shallow wells, U_0 can be described by the cubic approximation

$$U_0 = \frac{2}{3}\sqrt{1 - \beta^{-2}} E_J \epsilon^3, \quad (5)$$

where

$$\epsilon = \sqrt{2(\phi_c - \phi)/\sqrt{\beta^2 - 1}} \quad (6)$$

and $\phi_c = [\pi/2 + \sqrt{\beta^2 - 1} + \sin^{-1}(1/\beta)]$ is the external phase at which $U_0 = 0$. Since we ensure that the particle always starts in the upper well, we can write $P_{escape} = 1 - e^{-\Gamma \Delta t}$.

By repeating the measurement protocol many times and stepping the height of the applied flux pulse that controls the barrier, a probability curve of state occupation can be experimentally determined. The resulting probability curve is shown in Fig. 6. We define σ as a figure of merit describing the fidelity of the readout, which is the difference in flux Φ between $P_{escape} = 0.1$ and $P_{escape} = 0.9$. We show that our HyQUID readout implementation can
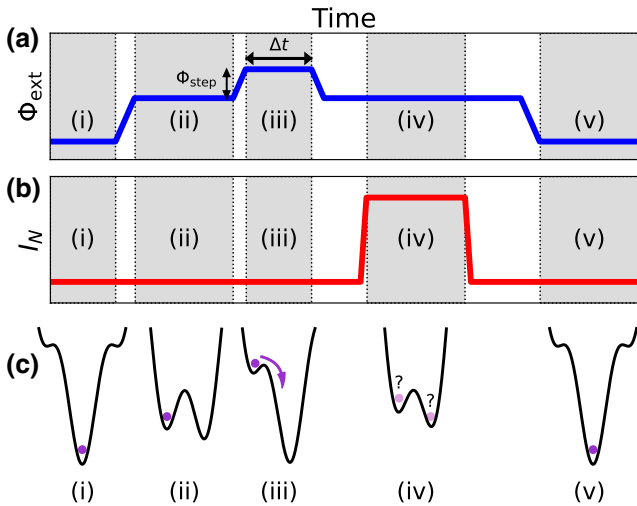

FIG. 5. The description of the pulsed-measurement protocol used to measure escape rates from the potential well of the system. (a) The blue line shows the applied flux Φ_{ext} as a function of time. (b) The red line shows the measurement current I_N through the vertical branch of the cross. (c) The protocol can be described by five regions, (i) through (v), with the energy potential shown for each region, as follows: (i) the system is initialized so that it sits in a lower well; (ii) the well is raised by increasing Φ_{ext}; (iii) a short flux pulse Φ_{step} is applied for time Δt, to temporarily lower the barrier. (iv) The barrier is reinstated by reducing Φ_{ext}—the HyQUID resistance is measured to determine if the system is in the upper or lower well; (v) the system is reset. The escape probability P_{escape} can be determined by repeating the process as a function of Φ_{step}.
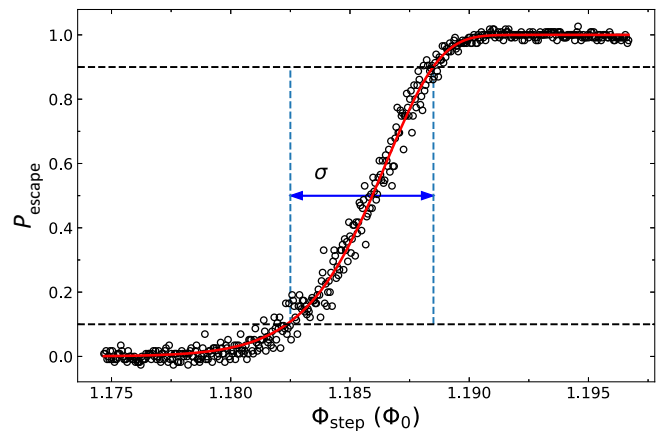

FIG. 6. The probability of escape as a function of the step height, measured according to the method described in Fig. 5 using a pulse length $\Delta t = 200$ μs. σ is a figure of merit describing the difference in Φ_{step} between $P_{escape} = 0.1$ and $P_{escape} = 0.9$. For this system, $\sigma = 0.006\Phi_0$.

detect changes in flux $\sigma = 0.006\Phi_0$. This resolution is comparable to that of the bifurcation amplifier used by Lupaşcu *et al.* to probe the state of a flux qubit [4].

2. Latching readout using bias current manipulation

The protocol shown in Fig. 7 uses the bias current I_N to control the potential well (by controlling β). One advantage of this protocol is that the applied flux is constant after initialization, which could be beneficial when the readout circuit is coupled to a flux-sensitive device such as a flux qubit. To estimate the performance of the HyQUID latching readout using the protocol shown in Fig. 7, we use experimentally determined probability curves for multiple fixed values of I_N. From the experimental data shown in Fig. 6, we fit the probability curve and extrapolate between probability curves measured at different values of I_N. This allows the simulation of a probability curve for the protocol shown in Fig. 7. The switching probabilities at two different values of the applied flux are shown in Fig. 8. We show two flux values $\Phi_{step} = 1.02\Phi_0$, and $\Phi_{step} = 1.01\Phi_0$. Following the convention from Siddiqi *et al.* [5], we define the discrimination power d as the maximum difference between the two switching-probability curves. The relative difference between the two curves can be described as $\Delta\Phi = 2(\Phi_2 - \Phi_1)/(\Phi_2 + \Phi_1)$. We find that
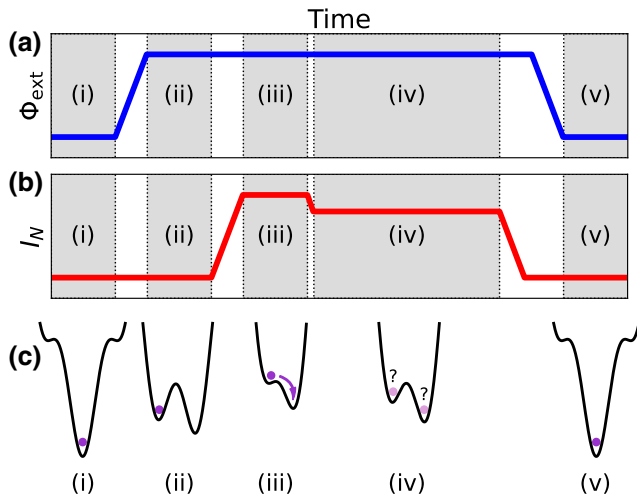

FIG. 8. The probability of escape as a function of the voltage applied across the normal reservoirs. We show curves of P_{escape} versus V_N corresponding to two flux positions. The curves are obtained using the experimental P_{escape} vs Φ_{step} curves, as shown in Fig. 6. We follow the convention of Siddiqi *et al.* [5] and describe the discrimination power d as the maximum difference between two switching-probability curves. For $\Delta\Phi/\Phi_0 = 1\%$, we find $d \approx 76\%$.

for $\Delta\Phi/\Phi_0 \approx 1\%$, $d = 76\%$. This is comparable to the performance described in Ref. [5].

IV. DISCUSSION AND CONCLUSION

The latching amplifier is suitable for probing the state of a superconducting qubit for a number of reasons. First, by correctly tuning the value of β, it is possible to make the magnetometer sensitive to extremely small changes in flux. Second, due to its latching action, the act of reading out the qubit can be separated from the act of probing the qubit, minimizing the back action. Third, by minimizing the mutual inductance between the flux-sensitive loop and the bias current and/or voltage leads (e.g., using a HyQUID with a folded-cross design as per Ref. [14]), the decoherence of the qubit by the measurement system can be minimized.

An important advantage of the HyQUID in bifurcation mode is that the screening Josephson current acts to reduce the thermal-flux noise $\delta\Phi_{th}$ introduced by the Nyquist noise in the S-N-S junction. In the absence of a Josephson screening current, the Nyquist thermal-noise current $\delta I_{th} = \sqrt{4k_BT\Delta f/R}$, where R is the resistance of the S-N-S junction in the normal state, introduces a current that circulates in the loop $\delta I_i = \delta I_{th}$. The thermal-flux noise in the loop is then given by

$$\delta\Phi_{th} = L\delta I_{th}. \tag{7}$$

This thermal-flux noise increases the noise floor, which reduces the sensitivity of the magnetometer and contributes to the back action of the readout.

FIG. 7. An alternative pulsed-measurement protocol to determine the escape probability. (a) The applied flux Φ_{ext} as a function of time. (b) The current I_N as a function of time. (c) Similar to Fig. 5, the protocol can be described by five regions, (i) through (v), with the energy potential shown for each region as follows: (i) the system is initialized so that it sits in a lower well; (ii) the well is raised by increasing Φ_{ext}; (iii) a short measurement current pulse is applied to temporarily lower the barrier; (iv) the barrier is reinstated by reducing the measurement current pulse—the HyQUID resistance is measured to determine if the system is in the upper or lower well; (v) the system is reset. The escape probability P_{escape} can be determined by repeating the process as a function of I_N.
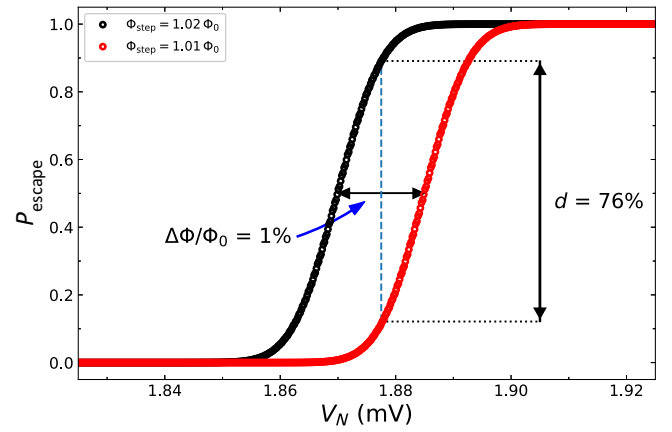
The Josephson supercurrent δI_s influences the current δI_i and partially screens the Nyquist current. The current circulating in the loop is $\delta I_i = \delta I_s + \delta I_{th}$ due to current conservation [14]. The value of δI_i can be determined by minimizing the energy of the loop [14,21]. The total energy of the loop is

$$W = W_k + W_m = \frac{L\delta I_i^2}{2} + \frac{L_k \delta I_s^2}{2}, \qquad (8)$$

where the first term describes the energy of the magnetic field due to the circulating current δI_i. The second term describes the kinetic energy due to the superconducting electrons in the normal branch of the HyQUID. The resulting thermal-flux noise is given by

$$\delta\Phi_{th} = \left(\frac{LL_k}{L+L_k}\right) I_{th}, \qquad (9)$$

where $L_k = \Phi_0/2\pi I_c$ is the kinetic inductance. Note that $\delta\Phi_{th} \to L_k I_{th} \to 0$ as $I_c \to \infty$; therefore, designing a HyQUID with a high critical current acts to reduces the flux noise induced by the interferometer, which can cause decoherence in the coupled qubit.

To further optimize the HyQUID for latching readout, we focus on the figures of merit σ and d. By examination of Eq. (5), we see that the value of $dU_0/d\Phi$ close to $\Phi = \Phi_0/2\pi$ should reach a maximum as $\beta \to 1$. Therefore, to minimize σ, the HyQUID should be operated close to this point. The performance of the HyQUID could therefore be improved by designing an interferometer with $1 > \beta > 1.5$ when $I_N = 0$. This could be achieved by adjusting the junction length $L_{c\text{-}d}$ and/or the HyQUID loop size. This would allow the HyQUID to operate at close to its optimal point using only a small bias current I_N through the resistive N branch reducing any heating effects. The response time of the HyQUID is estimated to be less than 40 ps [22]—fast enough to enable utilization of the HyQUID latching readout in typical qubit-readout protocols (see, e.g., Ref. [23,24]). The resistance of the normal part of the HyQUID can be changed by modifying the dimensions of the sample or by using materials with a higher resistivity. However, an impedance-matching circuit could be employed to match the impedance of the HyQUID with the characteristic 50 Ω impedance of microwave electronics.

To conclude, we present a hybrid quantum interference device that can be set in a bistable regime through *in situ* control of the Josephson screening current by application of a dc tuning current without entering the normal state. We show that in this regime, the HyQUID can be operated in a latching mode for quantum circuit readout. We employ a pulsed measurement to investigate the dynamics of the HyQUID in this mode and test the fidelity of the readout. The differential-resistance behavior as a function of either the flux or the current is in agreement with our modeling of the HyQUID dynamics.

We believe that this embodiment of the HyQUID is suitable for applications where high sensitivity and low back action are needed. In particular, we believe that the techniques described here could be applied to the readout of superconducting flux qubits.

The latching dynamics of the HyQUID may also have utility in superconducting logic architectures as a storage cell such as those proposed in Ref. [25], where a quantum state may be stored and then read out much later.

APPENDIX: TUNABLE HyQUID OPERATION

As discussed in the main text, the HyQUID operation regime can be tuned by varying the β screening parameter (by varying the critical current through application of a dc current between the two normal reservoirs). Figure 9 shows the oscillations of the differential resistance of the interferometer as a function of the applied flux Φ at different I_N-controlled β. At large β, periodic oscillations with regular sharp changes in the resistance as a function of the applied flux are seen showing hysteresis when the field sweep direction is reversed. The phase as a function of
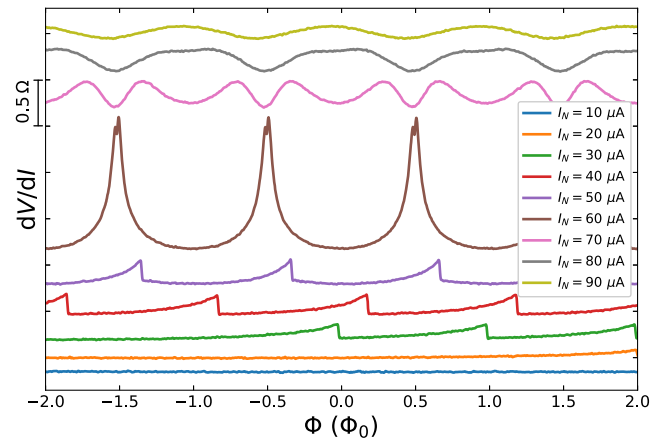

FIG. 9. (a) The differential resistance dV/dI (Ω) of the HyQUID as a function of the applied flux Φ at different bias currents I_N. The plots are offset on the y axis for clarity. Progression from the hysteretic regime (I_N large; I_c, β small) to the nonhysteretic regime (I_N small; I_c, β large) is clearly demonstrated.

flux at this value of β is multivalued. Initially, the superconducting phase starts on one branch where there is a relatively small gradient. As the flux approaches a critical value, the gradient changes sign. Past this critical flux, the gradient becomes negative. Values of phase on the negative gradient are unstable and so the phase jumps to the next branch, leading to the sudden switch seen in the magnetoresistance. This process is described in the main text and shown in Fig. 3.

As we increase I_N, the hysteresis disappears (it corresponds to the interferometer having $\beta < 1$). The relationship between the phase and the flux is no longer multivalued and R_N as a function of Φ is no longer path dependent [see Figs. 3(b) and 3(d)]. The transfer function $dV/d\Phi$ is maximized around $\Phi = \Phi_0/2$. Operation of the interferometer in this regime enhances the sensitivity with $dV/d\Phi = 1.92$ $\mu\mathrm{V}\Phi_0^{-1}$ (where V is the voltage measured by the lock-in amplifier across R_N) compared to 0.27 $\mu\mathrm{V}, \Phi_0^{-1}$ for a perfectly sinusoidal oscillation of the same amplitude.

At higher values of I_N, we observe a splitting of the peaks of the magnetoresistance oscillations and eventually a π shift in the phase of the oscillations. This is a consequence of the change in the differential resistance at higher measuring currents. A detailed explanation of this phenomenon can be found in Ref. [16].

[1] I. Chiorescu, Y. Nakamura, C. J. P. M. Harmans, and J. E. Mooij, Coherent quantum dynamics of a superconducting flux qubit, Science **299**, 1869 (2003).

[2] J. M. Martinis, M. Ansmann, and J. Aumentado, Energy Decay in Superconducting Josephson-Junction Qubits from Nonequilibrium Quasiparticle Excitations, Phys. Rev. Lett. **103**, 097002 (2009).

[3] J. Männik and J. E. Lukens, Effect of Measurement on the Periodicity of the Coulomb Staircase of a Superconducting Box, Phys. Rev. Lett. **92**, 057004 (2004).

[4] A. Lupascu, E. F. C. Driessen, L. Roschier, C. J. P. M. Harmans, and J. E. Mooij, High-Contrast Dispersive Readout of a Superconducting Flux Qubit Using a Nonlinear Resonator, Phys. Rev. Lett. **96**, 127003 (2006).

[5] I. Siddiqi, R. Vijay, F. Pierre, C. M. Wilson, M. Metcalfe, C. Rigetti, L. Frunzio, and M. H. Devoret, Rf-Driven Josephson Bifurcation Amplifier for Quantum Measurement, Phys. Rev. Lett. **93**, 207002 (2004).

[6] I. Siddiqi, R. Vijay, M. Metcalfe, E. Boaknin, L. Frunzio, R. J. Schoelkopf, and M. H. Devoret, Dispersive measurements of superconducting qubit coherence with a fast latching readout, Phys. Rev. B **73**, 054510 (2006).

[7] R. Vijay, M. H. Devoret, and I. Siddiqi, Invited review article: The Josephson bifurcation amplifier, Rev. Sci. Instrum. **80**, 111101 (2009).

[8] P. C. de Groot, A. F. van Loo, J. Lisenfeld, R. N. Schouten, A. Lupascu, C. J. P. M. Harmans, and J. E. Mooij, Low-crosstalk bifurcation detectors for coupled flux qubits, Appl. Phys. Lett. **96**, 123508 (2010).

[9] A. Lupascu, S. Saito, T. Picot, P. C. de Groot, C. J. P. M. Harmans, and J. E. Mooij, Quantum non-demolition measurement of a superconducting two-level system, Nat. Phys. **3**, 119 (2007).

[10] D. I. Schuster, A. Wallraff, A. Blais, L. Frunzio, R.-S. Huang, J. Majer, S. M. Girvin, and R. J. Schoelkopf, Ac Stark Shift and Dephasing of a Superconducting Qubit Strongly Coupled to a Cavity Field, Phys. Rev. Lett. **94**, 123602 (2005).

[11] A. P. Sears, A. Petrenko, G. Catelani, L. Sun, H. Paik, G. Kirchmair, L. Frunzio, L. I. Glazman, S. M. Girvin, and R. J. Schoelkopf, Photon shot noise dephasing in the strong-dispersive limit of circuit QED, Phys. Rev. B **86**, 180504(R) (2012).

[12] V. T. Petrashov, V. N. Antonov, P. Delsing, and T. Claeson, Phase Controlled Conductance of Mesoscopic Structures with Superconducting "Mirrors", Phys. Rev. Lett. **74**, 5268 (1995).

[13] V. T. Petrashov, K. G. Chua, K. M. Marshall, R. S. Shaikhaidarov, and J. T. Nicholls, Andreev Probe of Persistent Current States in Superconducting Quantum Circuits, Phys. Rev. Lett. **95**, 147001 (2005).

[14] C. D. Shelly, E. A. Matrozova, and V. T. Petrashov, Resolving thermoelectric "paradox" in superconductors, Sci. Adv. **2**, e1501250 (2016).

[15] A. F. Morpurgo, T. M. Klapwijk, and B. J. van Wees, Hot electron tunable supercurrent, Appl. Phys. Lett. **72**, 966 (1998).

[16] V. T. Petrashov, R. S. Shaikhaidarov, I. A. Sosnin, P. Delsing, T. Claeson, and A. Volkov, Phase-periodic proximity-effect compensation in symmetric normal/superconducting mesoscopic structures, Phys. Rev. B **58**, 15088 (1998).

[17] K. K. Likharev, *Dynamics of Josephson Junctions and Circuits* (Taylor & Francis, Philadelphia, 1986).

[18] J. Clarke and A. Braginski, *The SQUID Handbook: Fundamentals and Technology of SQUIDs and SQUID Systems* (Wiley, Weinheim, 2006).

[19] J. Kurkijärvi, Intrinsic fluctuations in a superconducting ring closed with a Josephson junction, Phys. Rev. B **6**, 832 (1972).

[20] A. G. Kofman, Q. Zhang, J. M. Martinis, and A. N. Korotkov, Theoretical analysis of measurement crosstalk for coupled Josephson phase qubits, Phys. Rev. B **75**, 014524 (2007).

[21] V. L. Gurevich, V. I. Kozub, and A. L. Shelankov, Thermoelectric effects in superconducting nanostructures, Eur. Phys. J. B—Condens. Matter Complex Syst. **51**, 285 (2006).

[22] C. Checkley, A. Iagallo, R. Shaikhaidarov, J. T. Nicholls, and V. T. Petrashov, Andreev interferometers in a strong radio-frequency field, J. Phys.: Condens. Matter **23**, 135301 (2011).

[23] R. Barends *et al.*, Superconducting quantum circuits at the surface code threshold for fault tolerance, Nature **508**, 500 (2014).

[24] F. Arute *et al.*, Quantum supremacy using a programmable superconducting processor, Nature **574**, 505 (2019).

[25] N. Ligato, E. Strambini, F. Paolucci, and F. Giazotto, Persistent Josephson phase-slip memory with topological protection, arXiv:2005.14298 [cond-mat.mes-hall] (2020).